High-Resolution Imaging of Objects in the Post-AGB to Planetary Nebula Transition

Judy Cheng
Department of Physics and Astronomy, Johns Hopkins University, Baltimore, MD 21218

ABSTRACT

We have obtained high-resolution images of two carbon-rich objects that are undergoing the transition from post-AGB star to planetary nebula: IRAS 21282+5050 (hereafter IRAS 21282), a young planetary nebula, and AFGL 3068, a post-AGB star with a high mass-loss rate.

Detailed structure is seen in IRAS 21282. A torus of dust, with its polar axis in the N-S direction, surrounds the central star, impeding the wind in the E-W direction. This has caused the nebula to develop elongation in the N-S direction. Immediately surrounding the central star is a cavity where the dust has been cleared out. Beyond this cavity is the ionization front, which marks the extent of the ionized region. The presence of a shock front slightly farther out is suggested by linear emission.

AFGL 3068 was observed in both infrared and optical wavelengths. Two different models are proposed to explain the presence of two point sources in the infrared images. The first hypothesis is that we are seeing a nebula surrounding the central star next to a reflection nebula. The second hypothesis is that the two point sources are two stars, which are responsible for the spiral structure seen in the optical wavelengths.

Subject headings: post-AGB stars, pre-planetary nebulae, IRAS 21282+5050, AFGL 3068

1. Introduction

For a star less than about eight solar masses, the end of its life is heralded by a period of extreme mass loss. As the star moves up the asymptotic giant branch (AGB), it sheds its outer layers until its hot core is exposed. Ultraviolet radiation from the core ionizes the surrounding medium, and the object becomes a planetary nebula. Many planetary nebulae have been observed in detail, revealing some with spectacular bipolar and multi-polar structures. Most such objects deviate from circular symmetry in a way that is consistent with predominant axisymmetry. These objects are no longer spherically symmetric like their progenitor stars and are described to be axisymmetric.

Not enough is known about the short transitional period between a post-AGB star and a evolved planetary nebula, most notably the mechanism behind the axisymmetric loss of mass, which is so prevalent in evolved planetary nebulae, but unseen in the post-AGB stage. By studying two objects still in this transitional period, we hope to gather some clues about how this axisymmetry occurs.

IRAS 21282+5050 (hereafter IRAS 21282) is a very young carbon-rich planetary nebula with a O7(f)-[WC11] Wolf-Rayet central star, in which ionization has only recently begun (Likkel et al. 1994), making it a good candidate for studying the early stages of a planetary nebula's evolution. It has been studied extensively at radio and infrared wavelengths. Shibata et al. (1989) observed the CO emission and described the object as an expanding torus with its polar axis directed E-W. Meixner et al. (1993) imaged the infrared polycyclic aromatic hydrocarbon (PAH) emission at 3.3, 11.3, and 12.5μm, and saw a toroidal structure as well, but contended that the polar axis was directed N-S, not E-W, for molecular emission. New data may be able to resolve this debate, as well as provide information on the more minute details of

this system.

AFGL 3068 (also called IRAS 23166+1655) is located at galactic coordinates $l = 93.5$ and $b = -40.4$ (Groenewegen et al. 2002). It is classified as an extreme carbon star having a very high mass loss rate, estimated to be anywhere from $\sim 1.5\times10^{-5}M_{\odot}$/yr (Winters et al. 1997) to $1.2\times10^{-4}M_{\odot}$/yr (Le Bertre et al. 1995). More recently, Woods et al. (2003) gave its mass-loss rate as $2\times10^{-5}M_{\odot}$/yr. The expansion rate of the dust has been determined to be $\sim$ 15km/s. Values published for the expansion velocity include 14km/s (Woods et al. 2003), 14.7km/s (Winters et al. 1997), and 15.1km/s (Groenewegen et al. 2002). It is believed to be a post-AGB star (or pre-planetary nebula), at the stage where axisymmetry is first developing. We have caught this object in this short-lived phase, and have been able to view it in several wavelengths at the highest resolutions available.

2. Data

High-resolution images of IRAS 21282 and AFGL 3068 were taken in July 2004 using the Near Infrared Camera 2 (NIRC2) at the Keck Observatory on Mauna Kea, Hawaii. Between three to ten different raw images were taken using each filter (listed in Table 1), with the source position shifted to different positions on the array. The diffraction-limited resolution of the telescope is 0.055" in the K-filter (2.196μm) and scales with wavelength. This process, called dithering, helps to ensure that good pixels are present in all locations of the image. Darks were taken to account for the counts from the dark current, an instrumental source of excess counts.

Each final image is made up of a combination of several individual raw images (1024 by 1024 pixel images produced by NIRC2), which were mosaicked and added after subtracting the sky background and the darks, and compensating for cosmic ray hits and bad pixels. The flat (in this case the normalized sky background) was obtained by finding the median of the images. Many steps were also taken to minimize the amount of noise in the reduced images. Cosmic ray hits were identified as pixels in the raw images that deviated more than 10-sigma from their neighbors. These pixels were set to equal the average of the surrounding pixels before the final addition of the images. A similar method was used in finding bad pixels, which were pixels in the flat that deviated by more than 6-sigma from their neighboring pixels. These pixels were set to zero and not included in the final addition. Hot pixels, those that deviated from the mean local level in the darks by more than 10-sigma, were treated in the same way. After these pixels were taken into account, the images were cross-correlated (to match up the location of the source in each image) and then added together. This process yielded the best possible image of the bright source on a negligible background. All data reduction on the NIRC2 images was done in IDL.

The data are not photometrically calibrated, because the Strehl ratios for the natural guide star adaptive optics observations are dependent on the variable atmosphere. The absolute fluxes have not been determined.

In addition to the Keck images, we had access to images of AFGL 3068 from the Advanced Camera for Surveys (ACS) in the Hubble Space Telescope (HST), which showed the object in optical wavelengths, 590.7 and 833.3 nm. These images were reduced by Raghvendra Sahai of the Jet Propulsion Laboratory.

2.1. IRAS 21282+5050

IRAS 21282 was imaged in filters ranging from 1.5804 to 4.670μm, and the results of the data reduction are shown in Figure 1. For two filters, Fe II and Br-γ, a narrow-band continuum image (H-continuum from Fe II, and K-continuum from Br-γ) was subtracted so that the images showed only the line emission from Fe II and Br-γ.

In each image, the central star is clearly visible, with bright regions to the East and West, which make up a surrounding torus of material. These images give support to the conclusion of Meixner et al. (1993), that the torus is aligned with its polar axis directed N-S.

The first four filters shown–H, K-continuum, L', and Ms–show the dust emission from the nebula, from short to long wavelength. For a blackbody object, the shortest wavelength arises predominantly from the hottest dust, and the longest wavelength from the coldest dust. The images at the longer wavelengths, emphasizing the emission from colder dust, show more extended emission,

TABLE 1
FILTERS

Object	Filter Name	Wavelength Ranges (μm)	Exposure Times (s)
IRAS 21282	H-continuum	1.5688-1.5920	500
	H	1.166-1.330	3000
	$H_2 v = 1 - 0$	2.1112-2.1452	500
	Fe II	1.6327-1.6583	500
	Br-γ	2.1523-2.1849	300
	K-continuum	2.2558-2.2854	400
	PAH	3.2627-3.3182	300
	L'	3.426-4.126	300
	Ms	4.549-4.790	210
AFGL 3068	H	1.485-1.781	1000
	K	2.028-2.364	900
	PAH	3.2627-3.3182	200

including emission along the N-S axis, suggesting that the dust temperature decreases with increasing distance from the central star. In these images, the emission extends about 5" in the N-S direction and 4" in the E-W direction. In the L' and PAH filters, thin line-like emissions are visible just inside the outer edge of the emission.

The one exception to this trend of increasing emission is the image taken using the Ms filter (4.670μm), which shows little detail compared to the other filters. One possible reason for this discrepancy is the presence of a carbon monoxide (CO) absorption line near 4.670μm, the central wavelength of this filter. The CO fundamental band is at 4.6-4.7μm. Likkel et al. (1994) observed CO emission in radio wavelengths, so we know that cold CO is present. This material may be responsible for absorbing the extended emission in the Ms filter.

To better see the structure of the nebula, we looked at several ratio images, which are shown in Figure 2. The ratio of K-continuum to H may indicate the distribution of the temperature. If the observed emission is due to dust, areas where H emission dominates, shown as the darker portions of the image, consist of hotter dust. This interpretation implies that the temperature decreases as one moves away from the central star. However, the presence of a cavity immediately surrounding the central star in all filters except for the H filter suggests that emission in the H-band may not be due to dust. One such possibility is Bremsstrahlung, or free-free emission.

The PAH to L' ratio accents the line-like emissions that we first observed in the individual PAH and L' filters. The PAH filter shows the distribution of excited PAH molecules within the system. There is a distinct boundary near the outer edges of the emission where PAH emission is relatively stronger than in the region surrounding the central star. Inside this boundary is a "cavity" where the more energetic "hard UV" radiation from the star has presumably destroyed the PAH molecules. The spatial band of stronger PAH emission immediately surrounding this cavity is where the ionizing radiation, in the form of "soft UV" radiation (at wavelengths longer than the Lyman limit, 912$\mathring{A}$), is exciting the molecules and emitting photons.

The ratio of Fe II to Br-γ also shows some of the structures present in this nebula. The Br-γ line is a recombination line, which occurs primarily in ionized regions. Fe II is used as a shock diagnostic. The torus, which is seen in each of the individual filters is observed in this ratio image as well, indicating the presence of ionized material close to the central star, whereas Fe II emission increases with distance. Although Fe II is used as a shock diagnostic, there do not appear to be Fe II-rich shocks present in this nebula. In this case, it is possible that the radiation field is ionizing iron more than once to Fe III and Fe IV, which would explain the relative lack of Fe II within the ionized region. Since Fe II can also be found in regions where there is molecular hydrogen, where no shocks are occurring, that would explain the presence of the increasing Fe II at the outer edges of the extended emission.

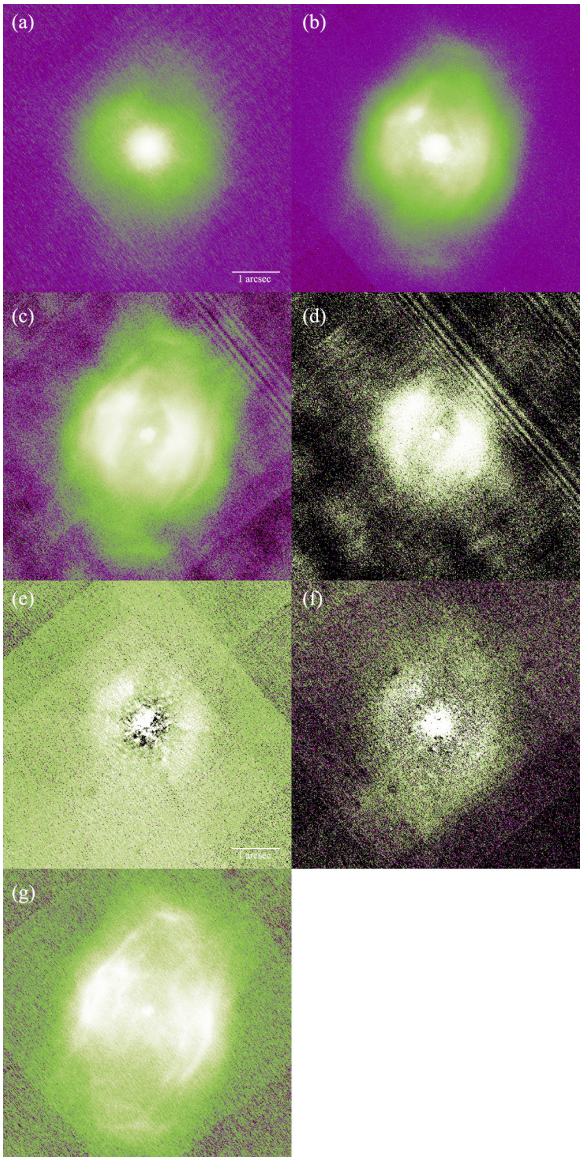

Fig. 1.— High-resolution images of IRAS 21282 from Keck: (a) H, 1.633μm; (b) K-continuum, 2.2706μm; (c) L', 3.776μm; (d) Ms, 4.670μm; (e) Fe II, 1.6455μm; (f) Br-γ, 2.1686μm; (g) PAH, 3.2904μm. Continuum images were subtracted from the Fe II and Br-γ data, so that only emission is seen in Figures 1(e) and 1(f).

2.2. AFGL 3068

This object was viewed in three different filters, 1.633, 2.196, and 3.2904μm, and the reduced images are shown in Figure 3. The H and K filters

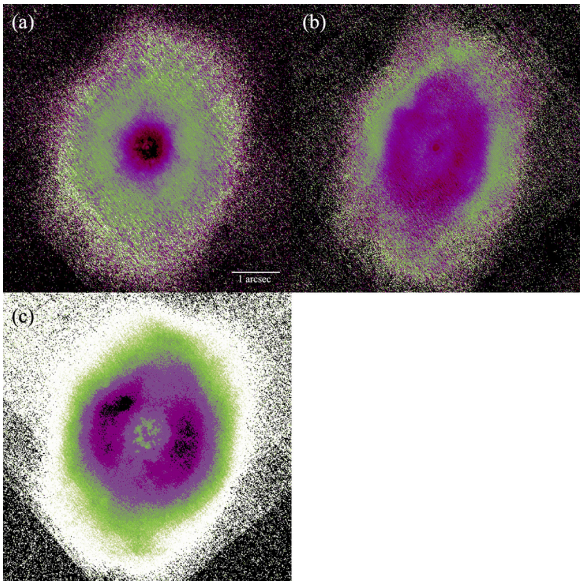

Fig. 2.— Ratio images: (a) K-continuum/H; (b) PAH/L'; (c) Fe II/Br-γ.

showed similar morphologies. Two point sources aligned approximately E-W were surrounded by approximately circular emission, with a radius of $\sim$ 1.5". While the peak of the eastern source is about five times brighter in the H-band, the peak of the western source is about two times brighter in the K-band. Only one point source is observed in the PAH-band, presumably the western point, which has a trend at shorter wavelengths of increasing brightness with decreasing wavelength. The FWHM of each of the peaks in the K-band are approximately 20 pixels, or $\sim$ 0.2". Given that the diffraction limit of this filter is 0.055", the two point sources are extended.

In the HST ACS image, a large spiral structure was seen centered at the coordinates of the star. The relative scales of the ACS and NIRC2 images are shown in Figure 4. This morphology of this spiral can be described as the result of a garden sprinkler" effect, where the mass-loss of the star is being gravitationally directed by a binary companion. As the companion orbits around the mass-losing star, the outflow is pulled toward the companion, resulting in a circular structure as the companion completes a revolution around the mass-losing star. The circles, however, do not close because of the outward expansion velocity of

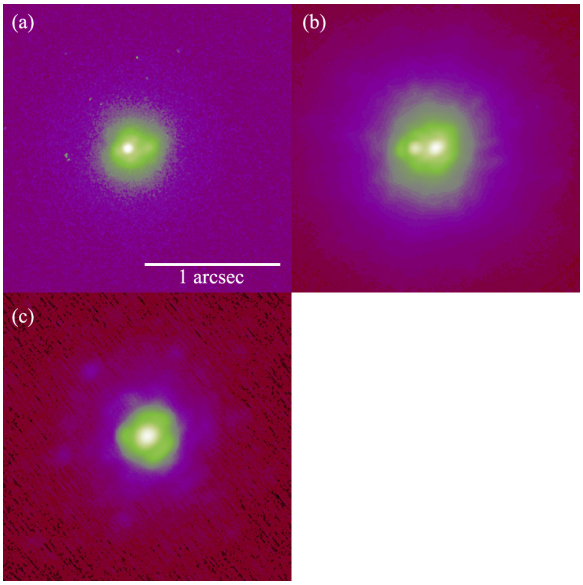

Fig. 3.— High-resolution images of AFGL 3068 from Keck: (a) H, 1.633μm; (b) K, 2.196μm; (c) PAH, 3.2904μm.

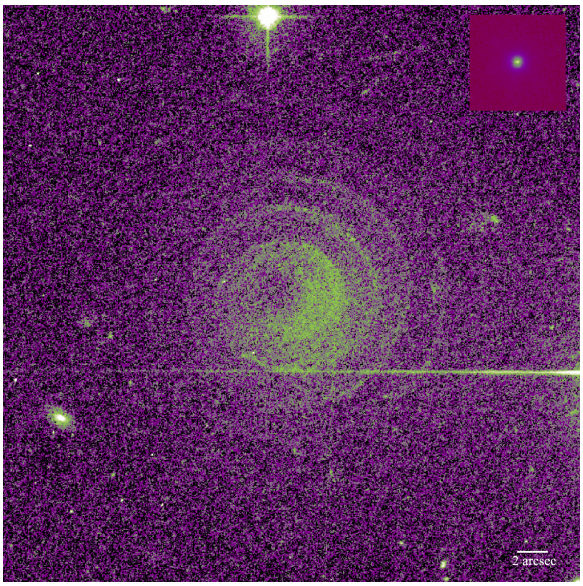

Fig. 4.— Optical image of AFGL 3068 from Hubble. Inset: Relative size of K-band emission.

the material.

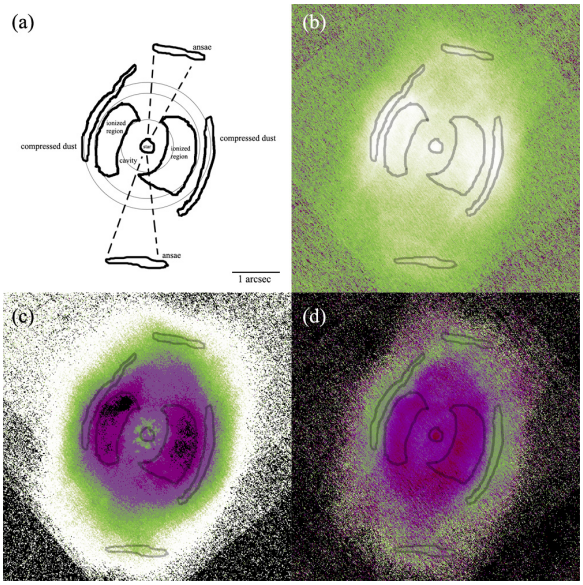

Fig. 5.— Schematic diagram of IRAS 21282: (a) The diagram, with main parts labeled. The diagram is then imposed on (b) PAH, (c) Fe II/Br-γ, and (d) PAH/L'.

3. Discussion

3.1. IRAS 21282+5050

Given this data, we can come up with a picture of what is happening in the system. A schematic diagram of the nebula is presented in Figure 5, with the main structures superimposed on three different images to show the relative scales. With an assumed distance of 2 kpc (Meixner et al. 1993), 1" is approximately equal to 1×10^9km. Immediately surrounding the central star is a cavity, about 0.6" in radius, where the high velocity winds from the hot core of the star have pushed the dust out of the way. The winds move through the cavity but are impeded by the torus of dust as it moves outward. The elliptical shape of the object is a result of the lack of dust in the N-S direction, which has allowed the winds to travel farther along the polar axis.

Two ansae, the small linear emission structures in the north and south edges of the nebula are observed in both the PAH and L' filters. The two ansae and the linear emissions beyond the torus suggest the presence of a shock front approximately 1.4" away from the central star, which is

compressing material as it moves outward. This is represented in Figure 3 by the largest of the concentric circles. Realistically, the shock front will deviate from the circle in the north and south directions (it will be farther away from the central star), but the circle is meant to serve as an indicator of where the shocks are occurring in the equatorial" regions of the nebula.

The shock front precedes the ionization front, indicated by the second largest circle, about 1.2" from the central star. This is the extent to which the ionization has occurred; material found beyond the ionization front is neutral. The ionized region is shown most definitively in the Br-γ image, as Br-γ is an indicator of where ionization has occurred.

The innermost circle shows the approximate size of the cavity, where the wind from the star has cleared out the bulk of the dust. From Figure 1, it can be seen that, with the exception of the H-band, there is no emission from the area immediately surrounding the central star. The emission in the H-band, then, may be explained with the presence of Bremsstrahlung (free-free emission) from the hot, inner nebula. The emission at 1.6μm is not from hot dust, but from radiation due to the acceleration of charged particles in a hot, thermal environment. Calculations of the emission coefficient must be done to determine the validity of this theory.

3.2. AFGL 3068

Initially, we thought that the presence of two bright sources was evidence of two lobes of a newly-appearing axisymmetric structure around the central star. In this scenario, the axisymmetry had not yet spread to the outer layers of dust, which were seen to be spherically symmetric. According to this hypothesis, the western point source would be the beginnings of a planetary nebula, while the eastern point source is a reflection nebula, which is seen as a result of Rayleigh scattering off of dust, for which the intensity of light is proportional to λ^{-4}. This kind of scattering is prevalent when the wavelength of the light is much larger than the size of the scatterers. This hypothesis, therefore, would account for the changing brightness of the eastern point since the reflection nebula is much brighter in the shorter wavelength H filter.

Another theory arose, however, when the ACS images revealed a spiral structure in the optical that was not seen in any of the infrared images (see Figure 5). The presence of circular arcs in AGB stars, pre-planetary nebulae, and planetary nebulae has been documented in previous publications. Sahai et al. (1998) imaged the Egg Nebula (CRL 2688, also carbon-rich with a high mass-loss rate) and noted the presence of a large number of round arcs" surrounding the center of the nebula. Hrivnak et al. (2001) observed arcs and rings around nine objects, including the Egg Nebula, at optical wavelengths and possible causes of the arcs were considered. They believed the arcs to be a common phenomenon in AGB stars and planetary nebulae, but had no definitive conclusions on how these arcs were formed. Explanations for the arcs ranged from a binary system, to instabilities in the mass-loss process of AGB stars, to the magnetic cycles of AGB stars.

In our analysis, we considered the possibility of a binary companion, where the gravity of one star directs the outflow of material from the mass-losing star. Systems similar to this one have been modeled by Mastrodemos and Morris (1999) for much closer binaries. Spiral structures surrounding Wolf-Rayet stars in binary systems have also been observed directly. In WR104 and WR98a, they observed "continuous spiral plumes of dust, formed by colliding winds" (Monnier et al. 2002).

In this scenario, the two sources seen in the images were not two lobes of a nebula, but a binary star system. To test this hypothesis, we first determined the period of the optical spiral structure, assuming an expansion velocity of 15.1km/s, and a distance of 1kpc (Groenewegen 2002). From the ACS image, we found a distance of about 2" between the crests of the spiral, which at a distance of 1kpc translated to 3×10^{11}km. At an expansion velocity of 15.1km/s, the period was calculated to be $\sim$ 600yrs.

Using Newton's form of Kepler's third law,

$$T^2 = \frac{4\pi^2 a^3}{G(M_1 + M_2)} \quad (1)$$

where $G = 6.67\times10^{-11}\mathrm{m}^3/\mathrm{kgs}^2$, we can then use the period of the spiral to determine how far apart the stars must be. We assume that the mass of each star was between one and two solar masses, which is in agreement with the value of one solar

mass used in Winters et al. (1997). Taking the two limiting cases (two $1M_\odot$ stars or two $2M_\odot$ stars) we find the combined masses of the two stars to be between two and four solar masses. With these values, Newton's law yields an expected separation of 0.09-0.12" between the two stars. This can be compared to the distance measured between the two point sources in the NIRC2 image, ~ 0.11".

The FWHM of the two sources in the K filter is ~ 0.2", which much larger than the diffraction limit at that wavelength, 0.055". Since the sources are extended, we are not simply seeing two stars. We may be seeing two stars surrounded by dust or a nebula surrounding the central star next to a reflection nebula.

However, this hypothesis raises some questions that are not easily answered. First, how likely is it that we would see two stars in the same evolutionary stage? Because the superwind phase is so short-lived (only about 10,000 years) compared to a star's lifetime, it is not very likely that two stars of equal or comparable mass will be in the same evolutionary stage at the same time. Also, the binary system does not explain why one point source is brighter in the H-band, while the other is brighter in the K-band. The reflection nebula theory explains this phenomenon well with Rayleigh scattering. Both models are still being considered.

4. Conclusion

In this study we observed two objects in the transition from post-AGB star to planetary nebula. IRAS 21282 has recently become a planetary nebula and is interesting as an example of the result of the transition into axisymmetry. In this nebula, a torus of dust is seen to impede outflow in the E-W direction, allowing material to travel farther in the N-S direction, causing the object's elongated appearance. We also observed the ionization front that is preceded by a shock front, which is suggested by the presence of a compressed dust layer.

AFGL 3068 is an object at the very beginning of the transitional stage. Two point sources were observed in the center of this object, but we have not yet been able to determine their nature. One idea is that one source, which is brighter at longer wavelengths, is an emission nebula surrounding the central star, while the other, which is brighter in shorter wavelengths, is a reflection nebula, which is brighter in the shorter because of the Rayleigh scattering. Another idea arose from the spiral structure that we observed in the optical. The spiral suggested the presence of a binary companion. Calculations of the period yielded a value for the separation of the two stars consistent with the distance observed between the two point sources in the infrared image. However, this hypothesis does not explain the changing brightnesses of the points in the infrared. More data on these objects will have to be gathered to make a more definitive conclusion.

REFERENCES

Groenewegen M. A. T., Sevenster M., Spoon H. W. W., Perez I., 2002, AA, 390, 511-522.

Hrivnak B. J., Kwok S., Su K. Y. L., 2001, ApJ, 121, 2775-2780.

Le Bertre T., Gougeon S., Le Sidaner P., 1995, AA, 299, 791-802.

Likkel L., Morris M., Kastner J. H., Forveille T., AA, 1994, 282, 190-196.

Mastrodemos N., Morris M., 1999, ApJ, 523, 357-380.

Meixner M., Skinner C. J., Temi P., Rank D., Bregman J., Ball J. R., Keto E., Arens J. F., Jernigan J. G., 1993, ApJ, 411, 266-273.

Monnier J. D., Tuthill P. G., Danchi W. C., 2002, ApJ, 567, L137-L140.

Sahai R., Trauger J. T., Watson A. M., Stapelfeldt K. R., et al., 1998, ApJ, 493, 301-311.

Shibata K. M., Tamura S., Deguchi S., Hirano N., Kemya O., Kasuga T., 1989, ApJ, 345, L55-L58.

Winters J. M., Fleischer A. J., Le Bertre T., Sedlmayr E., 1997, AA, 326, 305-317.

Woods, P. M., Schoier F. L., Nyman L. A., Olofsson H., 2003, AA, 402, 617-634.

This 2-column preprint was prepared with the AAS LaTeX macros v5.2.